Received: 14 May 2018 | Revised: 22 December 2018 | Accepted: 27 December 2018

DOI: 10.1111/pce.13516

ORIGINAL ARTICLE

WILEY Plant, Cell & Environment

Anatomical changes with needle length are correlated with leaf structural and physiological traits across five *Pinus* species

Na Wang[1,2] | Sari Palmroth[2] | Christopher A. Maier[3] | Jean-Christophe Domec[2,4] | Ram Oren[2,5]

[1] School of Forestry, Northeast Forestry University, Harbin 150040, China

[2] Nicholas School of the Environment, Duke University, Durham, NC 27708, USA

[3] Southern Research Station, USDA Forest Service, Durham, NC 27709, USA

[4] Bordeaux Sciences Agro, UMR 1391 INRA-ISPA, 33175 Gradignan Cedex, France

[5] Department of Forest Sciences, University of Helsinki, Helsinki, Finland

Correspondence
Sari Palmroth, Nicholas School of the Environment, Duke University, Durham, NC 27708, USA.
Email: sari.palmroth@duke.edu

Na Wang, School of Forestry, Northeast Forestry University, Harbin 150040, China.
Email: wangnsilv@163.com

Funding information
National Science Foundation, Grant/Award Number: NSF-IOS-1754893; Erkko Visiting Professor Programme of the Jane and Aatos Erkko 375th Anniversary Fund, through the University of Helsinki

Abstract

The genus *Pinus* has wide geographical range and includes species that are the most economically valued among forest trees worldwide. Pine needle length varies greatly among species, but the effects of needle length on anatomy, function, and coordination and trade-offs among traits are poorly understood. We examined variation in leaf morphological, anatomical, mechanical, chemical, and physiological characteristics among five southern pine species: *Pinus echinata*, *Pinus elliottii*, *Pinus palustris*, *Pinus taeda*, and *Pinus virginiana*. We found that increasing needle length contributed to a trade-off between the relative fractions of support versus photosynthetic tissue (mesophyll) across species. From the shortest (7 cm) to the longest (36 cm) needles, mechanical tissue fraction increased by 50%, whereas needle dry density decreased by 21%, revealing multiple adjustments to a greater need for mechanical support in longer needles. We also found a fourfold increase in leaf hydraulic conductance over the range of needle length across species, associated with weaker upward trends in stomatal conductance and photosynthetic capacity. Our results suggest that the leaf size strongly influences their anatomical traits, which, in turn, are reflected in leaf mechanical support and physiological capacity.

KEYWORDS

conductance, leaf structure, leaf traits, nitrogen, photosynthesis, pine, plant hydraulics, stomata, water relations, xylem transport

1 | INTRODUCTION

Leaf size exhibits great plasticity, both along environmental gradients and within communities, varying by over 100,000-fold among species worldwide (Milla & Reich, 2007; Wright et al., 2017). Corner's hypothesis states that, compared with tree species with smaller leaves, species with large leaves have greater proportions of their shoot biomass invested in foliage and hold more widely spaced leaves on shoots (Corner, 1949). Thus, species with large leaves tend to experience less self-shading within a shoot (Falster & Westoby, 2003). Leaf size affects, or is related to, many functional traits. Combined with leaf organization on shoots, leaf size affects light interception efficiency and the net carbon assimilation capacity of a plant, in part by affecting the leaf boundary-layer conductance and thus water loss rate and leaf temperature (Yates, Verboom, Rebelo, & Cramer, 2010). Furthermore, leaf size affects plant productivity and adaptive capacity to changes in its environment (Pickup, Westoby, & Basden, 2005; Westoby, Falster, Moles, Vesk, & Wright, 2002; Wright, Falster, Pickup, & Westoby, 2006). A better understanding of constraints on the structural design of leaves, and the resulting coordination or trade-offs among leaf traits across species, is key to understanding variation of plant growth rates and adaptive and competitive capabilities.

The genus *Pinus* has a wide geographical range and includes species that are the most economically valued among forest trees worldwide (Wear & Greis, 2002). Among conifers, pines species show the largest range of needle length, yet relatively little is known about

the influence of needle length on needle structure and function and how variations in anatomical traits affect mechanical and physiological traits. More is known about how needle length and organization affect light distribution on needle surfaces (Niinemets, Tobias, Cescatti, & Sparrow, 2006; Stenberg, Palmroth, Bond, Sprugel, & Smolander, 2001; Thérézien, Palmroth, Brady, & Oren, 2007). The amount of light intercepted by unit of leaf area depends on its location relative to other shading elements in the canopy. In coniferous canopies, three-dimensional foliage elements are grouped into shoots, that is, (semi-) annual growth units, often considered the basic functional units. The mean light intensity, or mean irradiance, on needle surfaces of a shoot depends on the amount of light reaching the shoot and on the shoot interception efficiency. This efficiency varies with the size and orientation of the shoot and the dimensions and organization of the needles (Niinemets, Tobias, et al., 2006; Stenberg et al., 1994). *Ceteris paribus*, the mean shoot silhouette-to-total leaf area ratio ($\overline{STAR}$; Stenberg et al., 1994) first increases with needle length, reaching a maximum and decreasing thereafter with further increases in length (Figure 1a, simulated using the model by Thérézien et al., 2007). This simplified analysis does not account for other shoot structural characteristics, which vary among species, yet suggests a hypothesis that directly links needle length to irradiance on needle surfaces. That is, in a given light environment, mutual shading among needles of a shoot (inversely related to $\overline{STAR}$) $\overline{STAR}$ appears to reach a minimum at intermediate needle lengths, providing the highest mean irradiance on needle area relative to shoots with either shorter or longer needles. If light availability was the main driver of photosynthetic capacity and related leaf traits, these traits should show a similar pattern with needle length among species.

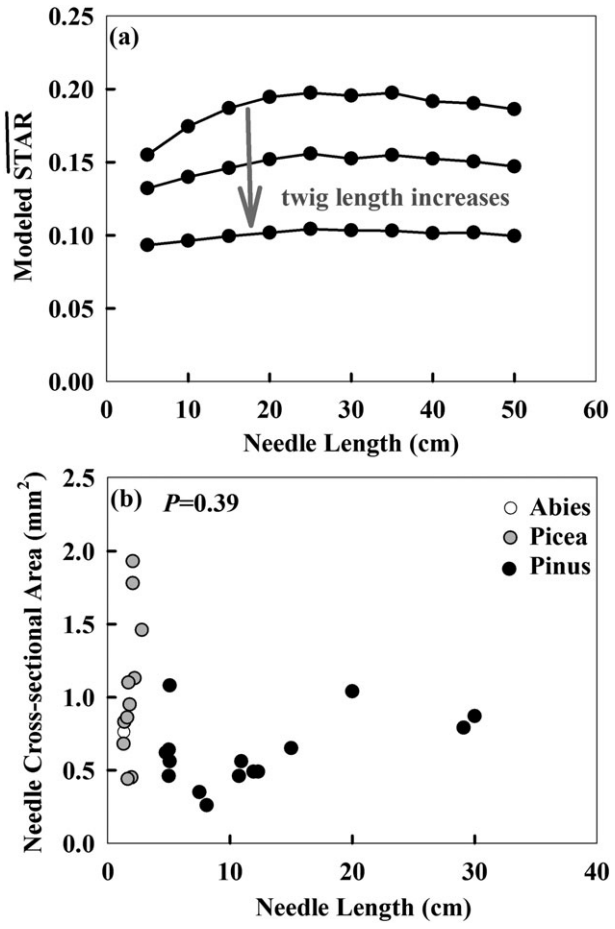

FIGURE 1 Variation in modelled spherically averaged shoot-silhouette-to-total-leaf-area ratio ($\overline{STAR}$; a), and needle cross-sectional area (b) with needle length. The model used in (a) is from Thérézien et al. (2007). The data in (b) were taken from published papers listed in Table S1

However, mechanical traits control the physical response of leaves to environmental forces, with physiological and ecological consequences (Niklas, 1999). Needles work as cantilevered mechanical "devices," bearing a relatively uniform load along their length. They must be sufficiently rigid to support their own weight mechanically against the pull of gravity yet flexible enough to bend or twist without breaking when subjected to strong and dynamic external forces, such as wind, snow, hail or ice formation, animal action, abrasion against other canopy elements, and falling debris (Raupach & Thom, 1981; Vogel, 1989). Previous studies demonstrated that the investment in support biomass (midrib and petiole mass) per unit leaf area (or leaf fresh mass) in larger leaves is greater than in smaller leaves (Niinemets, Portsmuth, & Tobias, 2006). In conifers, the bending force operating on a needle is proportional to the cube of its length (Niklas, 1992, 1999); thus, the biomass or volume fraction of supporting tissues (epidemical tissue plus xylem) must scale exponentially with needle length to maintain a given needle angle. However, among pine species, needle cross section does not increase with increasing needle length (Figure 1b, Table S1). This suggests that the extra structural support required for longer needles is not achieved simply through increased cross-sectional area and associated strength but by increasing the relative investment in mechanical tissues.

The hydraulic costs and benefits of deploying a given leaf area as many small versus fewer large leaves are still a matter of debate (Corner, 1949; Givnish, 1984; Niinemets, Portsmuth, & Tobias, 2006; Yang, Li, & Sun, 2008). The pathway of water within leaves represents a substantial portion of the whole-plant resistance to water flow from root to the substomatal air space (Nardini & Salleo, 2000; Sack & Holbrook, 2006). Thus, for example, correlations have been noted among leaf hydraulic conductance (K_{leaf}), maximum stomatal conductance (maximum g_s), transpiration, and photosynthetic rates across species (Brodribb, Feild, & Jordan, 2007; Sack, Cowan, Jaikumar, & Holbrook, 2003; Sack & Holbrook, 2006), with additional variation caused by resource availability (Domec et al., 2009; Sellin, Sack, Õunapuu, & Karusion, 2011). In angiosperms, K_{leaf} varies independently of leaf size among species because of the overwhelming effects of the great phylogenetic and developmental diversity of the vascular architecture (Sack et al., 2003; Sack & Frole, 2006). In contrast to the complex leaf vein patterns in angiosperm, pine needles have a very simple design that consists of a single middle vein (Esau, 1977; Zwieniecki, Stone, Leigh, Boyce, & Holbrook, 2006). However, whether the diversity in needle length translates to large differences in water transport capacity and, thus, in stomatal conductance and gas exchange remains unclear.

The hydraulic conductance of xylem, and along the flow paths outside the xylem to evaporation sites, largely depends on the dimensions and anatomy of the leaf (Brodribb et al., 2007; Scoffoni et al.,

2016). Unknown at this time, however, is whether variation among species in needle length is accompanied by variation in the anatomical properties of the xylem and of tissues outside the xylem (transfusion and mesophyll) and how these variations translate to differences in leaf function. These differences could manifest in variation of traits such as the hydraulic conductance of outside-xylem pathway ($K_{outside\text{-}xylem}$), xylem (K_{xylem}), or their composite, K_{leaf}, which represents the whole-leaf water transport capacity. For example, although needle cross-sectional area remains relatively constant with needle length (Figure 1b), the volume fraction of mechanical tissues could increase with length, forcing a reduction in the fraction of mesophyll tissue, along with the path length within the mesophyll, potentially decreasing the hydraulic resistance along the radial outside-xylem pathway. This could increase $K_{outside\text{-}xylem}$ and thus K_{leaf} with needle length (Brodribb et al., 2007; Domec, Palmroth, & Oren, 2016; Scoffoni et al., 2016) and the photosynthetic rate, if it is conductance limited. However, if it is limited by the amount of photosynthetic machinery per unit of area (e.g., the ratio of mesophyll cell surface area to leaf surface area; Nobel, Zaragoza, & Smith, 1975) and/or by mesophyll diffusion conductance (Kuusk, Niinemets, & Valladares, 2018b), such adjustments may reduce photosynthetic rates.

With increasing (average) light availability, the amount of photosynthetic machinery and biochemical demand for CO_2 (photosynthetic capacity) increase, along with the evaporative force driving transpiration, and must be met by an enhanced supply of CO_2 and liquid water through higher K_{leaf} and g_s (Brodribb et al., 2007; Scoffoni et al., 2016). Thus, needle length may affect both the mean irradiance on needle surfaces, as well as the hydraulic capacity for liquid water delivery required to keep stomata open, facilitating the use of captured solar energy in photosynthesis. This study aims at assessing the combined effect of needle length on variables that affect both leaf display to light and hydraulic capacity and the consequences to stomatal conductance and photosynthetic rate.

We studied the five most common pine species native to the south-eastern United States, namely, *Pinus echinata*, *Pinus elliottii*, *Pinus palustris*, *Pinus taeda* (two families), and *Pinus virginiana*, exhibiting a wide range in needle length. Except for *P. virginiana*, a member of subsection *Contortae*, the others are called "southern pines" (subsection *Australes*). All five species are shade intolerant, and among them, *P. palustris* is the least, and *P. virginiana* is the most shade tolerant. All five species are relatively well adapted to poor soils and show overlapping geographical ranges, each with at least two others. The evolutionary relationships of the southern pines remain unresolved (Koralewski, Mateos, & Krutovsky, 2016), and in this study, we assess leaf trait values of these co-occurring and related species as independent solutions to match energy capture by leaf surfaces with water supply to stomata. We aimed at exploring the potential mechanisms by which needle length affects leaf gas exchange in response to structural and hydraulic adjustments. We examined the variation in anatomical, mechanical, chemical, hydraulic, and gas exchange traits with needle length among the five species, growing under the same climatic and edaphic forcing. We hypothesize that the volume fraction of mechanical tissue (epidermal tissue plus xylem) would scale with needle length (H1a), whereas the fraction of mesophyll tissue and, consequently, the outside-xylem and leaf hydraulic resistances would decrease with needle length (H1b). Driven by the increase in leaf hydraulic conductance, stomatal conductance and maximum photosynthetic rates would also increase with needle length (H1c). However, if the variation of light availability on needle surfaces, induced by shoot structure through varying needle length (Figure 1a), was the main driver of photosynthetic capacity and related leaf traits, the relationship between leaf gas exchange characteristics and needle length would be concave as the amount of light on needle surfaces (relative to available light) declines at the higher portion of the range in needle length (H2).

2 | MATERIALS AND METHODS

2.1 | Site description

In 2011, 1-year-old seedlings of *P. echinata* Mill., *P. elliottii* Engelm., *P. palustris* Mill., *P. taeda* L. (two families), and *P. virginiana* Mill. were planted in 32 m × 40 m plots, with 4 m × 2 m spacing, on a site with sandy loam soil of the Appling series in the Duke Forest, Durham, NC (36°01′N, 78°59′W). *P. echinata* and *P. elliottii* plots were planted with the second-generation seedlings from Flint River Nursery, Byromville, GA. *P. palustris* seedlings are of various provenances across the south-eastern United States (Longleaf Pine Regional Provenance/Progeny Trial, NC State University Cooperative Tree Improvement Program and USDA Forest Service, Raleigh, NC). *P. taeda* seedlings are from two mass-control pollinated families (ArborGen, Inc., Ridgeville, SC), with broad (AGM-37) and narrow (AGM-22) crown characteristics, from Supertree Nursery, Blenheim SC. *P. virginiana* seedlings were from Claridge Nursery, Goldsboro, NC. At the end of the 2016 growing season, the dominant heights of the trees were as follows: *P. taeda*, 6.6 m; *P. elliottii*, 4.4 m; *P. virginiana*, 3.9 m; and *P. echinata*, 3.3 m. *P. palustris* trees showed a large range of heights due to the distinctive developmental pattern of the species (averaging 1.4 m in our plot), but the individuals sampled had passed the grass and "bottlebrush" stages and were ~2-m tall in the fall of 2015. The climate of the region is warm and humid with mean annual temperature of 15.5°C. Annual precipitation is 1,145 mm and distributed evenly throughout the year.

2.2 | Hydraulic measurements

Hydraulic measurements were conducted in October 2015 on branches collected from the upper crowns of five randomly sampled individuals per species (n = 5). To prevent pine resin from causing extraneous surface resistance through resin canal breakages, we soaked the end surfaces in water for 60 to 90 min before the first measurements to remove excess resin and then carefully recut the end-surfaces with a clean razor blade (Booker, 1977; Melcher et al., 2012). We describe below hydraulic resistance (R) rather than hydraulic conductance (K, e.g., R_{leaf} rather than $K_{leaf} = 1/R_{leaf}$), because resistances add in series, enabling measured values to be partitioned into their resistance components. The methodology used in this study is described in detail elsewhere (Domec et al., 2016). Briefly, leaf hydraulic resistance (R_{leaf}) was measured by a high-pressure flow metre

(HPFM; Tsuda & Tyree, 2000). Apical branches were connected to the HPFM (Dynamax Gen2, IN) with a water tight seal. Deionized, degassed water, filtered at 0.1 μm, was forced at a pressure of 0.2–0.3 MPa into the shoots through the stem and eventually out through the stomata. Temperature was automatically recorded by the HPFM, and all measurements were corrected to values at 25°C. Branch hydraulic resistance (R_{branch}) was shown to increase during the first 3–5 min, and data points were recorded every 30 s after the flow rate became stable. After R_{branch} was measured, the needles were removed with a fresh razor blade at their connections to the woody stem and the hydraulic resistance reassessed (R_{stem}). Because shoot resistances are added in series, R_{leaf} was calculated as $R_{leaf} = R_{branch} - R_{stem}$.

Hydraulic resistance was measured on both control (intact) leaves and on frozen and then thawed needles. Freezing the needles removes most of the hydraulic resistances of the outside-xylem water pathway (Cochard, Froux, Mayr, & Coutand, 2004; Domec et al., 2016; Nardini, Salleo, & Raimondo, 2003; Tyree, Nardini, & Salleo, 2001), and R_{leaf} estimated from such needles represents that of the leaf xylem water pathway (R_{xylem}). To estimate R_{xylem}, which represents the inverse of the axial leaf xylem conductance, we measured R_{branch} and R_{leaf} on frozen–thawed branches (frozen at −55°C for 10 min, and then thawed for 30 min at +23°C). Preliminary tests on four shoots showed that, in fact, 15 min was sufficient to completely thaw the samples because the branches were plunged in water at room temperature before connecting to the HPFM and that R_{branch}, once stable, remained so for >20 min, the period during which removing needles and remeasuring were completed (Domec et al., 2016). It should also be noted that, in our experiments, the freeze–thaw process did not cause embolism because thawing did not occur under tension (Pittermann & Sperry, 2006). Hydraulic resistance of the pathway outside the leaf xylem, the extravascular leaf resistance, was calculated as $R_{outside\text{-}xylem} = R_{leaf} - R_{xylem}$. Finally, we converted resistance to conductance, normalizing all hydraulic conductance values by the total needle surface area of the branch.

2.3 | Leaf structure and anatomy

In March 2017, needles were sampled from randomly assigned trees (five needles per tree and five trees per species) for structural and anatomical measurements. Samples were placed in plastic bags, transported to laboratory, and kept in a cold room until processing (within hours from collection). Free-hand transverse sections (with thickness of ~40 μm) of fresh needles were cut in the midsections of the samples using fresh razor blades. Sections thicker than 100 μm approach mesophyll cell size and may lead to erroneous estimates of some measures. The sections were photographed at 40×, 100×, and 400× magnification by a digital camera mounted on a microscope, and the images were analysed using the Motic Images Advanced 3.2 software (Motic Corporation, Zhejiang, China). Images taken at 40× were used to determine cross-sectional width, thickness, circumference (C), needle cross-sectional area, epidermal tissues area, and mesophyll area ($S_{mesophyll}$). Images taken at 100× were used to determine the area of central cylinder, vascular bundle, and transfusion tissue. Thickness of mesophyll tissue and area and circumference of individual mesophyll cells ($S_{mesophyll\ cell}$, $C_{mesophyll\ cell}$) were also recorded. Images taken at 400× were used to determine the xylem and phloem areas and the number and size of tracheids within the xylem area. From these measurements, mesophyll cells surface area ($S_{mesophyll\text{-}surf.}$) per needle surface area (S_{needle}) was calculated as $S_{mesophyll\text{-}surf.}/S_{needle} = (S_{mesophyll}/S_{mesophyll\ cell}) \times C_{mesophyll\ cell}/C$. Xylem hydraulic diameter was calculated as $\sum_{i=1}^{n} d_i^5 / \sum_{i=1}^{n} d_i^4$, where d is the diameter of the ith tracheid and n is the number of the tracheids in the xylem (Kolb & Sperry, 1999). In our study, mechanical (or supporting) tissue was defined as epidermal tissues plus xylem; therefore, mechanical tissue fraction (%) was calculated as the ratio of the sum of epidermal tissues area and xylem area to needle cross-sectional area.

To estimate dry/fresh mass ratio, dry (and fresh) density of needles, leaf mass per unit area, and leaf mass per unit length, three needle samples (made of 20–30 needle fascicles each) per tree from five trees per species were collected. Dry/fresh mass ratio was calculated as the ratio of needle dry mass to needle fresh mass. Dry and fresh density was calculated as the ratio of needle dry and fresh mass, respectively, to needle fresh volume. Leaf mass per unit area was calculated as the ratio of needle dry mass to total needle surface area ($LMA_{total\text{-}surf.}$, g m^{-2}). Leaf mass per unit length was calculated as the ratio of needle dry mass to total needle length (g m^{-1}). Fresh mass of needles was obtained, followed by fresh needle volume based on water displacement method. After drying the surface of the needles with a paper towel, needles were scanned. Projected area and needle length were estimated by analysing the images with the software Image-J (National Institutes of Health, MD). Total surface area was calculated as projected area × π following empirical studies demonstrating that the ratio is not significantly different from that quantity (Johnson, 1984; 3.08 ± 0.21 *SD* for six pine species, including *P. taeda* and *P. virginiana*; Oker-Blom & Smolander, 1988; 3.00 ± 0.28; Oker-Blom, Kaufmann, & Ryan, 1991; 3.09 ± 0.33). Finally, needles were oven dried at 65°C for 48 hr to a constant mass and weighed again.

2.4 | Gas exchange measurements

Gas exchange was measured during two campaigns in 2017. On April 26th–27th, light-saturated photosynthetic rates (A) and corresponding stomatal conductance (g_s) of 1-year-old needles on intact upper-crown branches were measured using three Li-Cor 6400 gas exchange system (with 6400-02B red/blue light source, and 20 × 30 mm chamber; Li-Cor Biosciences, Lincoln, NE). Ten trees ("gas exchange trees") of each species were randomly selected, and one set of measurements was taken from each tree (n = 10). Midsections of two to three sun-acclimated fascicles were enclosed in the chamber. After an acclimation period of a few minutes, until steady gas exchange rates were reached, we recorded the readings at 30-s intervals for 5 min. Chamber conditions were maintained close to ambient conditions. That is, (block) temperature were set to near ambient temperature (around 28°C during these 2 days) and quantum flux density to 1,800 μmol m^{-2} s^{-1}. We did not control water vapour pressure in the chamber, and the relative humidity ranged from 50% to 70%.

On June 2nd–4th and 8th–10th, photosynthetic responses to variations in leaf internal CO_2 concentration, that is, A–C_i curves, were measured. Curves were developed on 1-year-old foliage of detached shoots collected from five of the ten gas exchange trees (n = 5). The cut branches were recut under water and kept well hydrated during the measurements. For each sample, a single curve over 11 chamber CO_2 concentrations (400, 50, 100, 150, 200, 300, 400, 800, 1,000, 1,200, and 1,500 ppm) was measured. Other environmental variables in the chamber were maintained as described above. Maximum rates of carboxylation ($V_{c,\ max}$) were determined at a standard temperature of 25°C for each needle sample with the Farquhar biochemical model of photosynthesis (Farquhar, von Caemmerer, & Berry, 1980) as described by Medlyn et al. (2002) and the Rubisco kinetic characteristics obtained from Bernacchi, Singsaas, Pimentel, Portis, and Long (2001). We did not correct gas exchange rates for chamber diffusion leaks (Rodeghiero, Niinemets, & Cescatti, 2007). However, all our measurements were carried out with settings that minimize the leaks, that is, in humid field conditions, and with chamber conditions set close to ambient conditions (excluding $[CO_2]$ for A–C_i curves). Moreover, because the cross-sectional dimensions were fairly similar among the species in our study (Table 1), we assumed that the effect of any unavoidable leaks on $V_{c,\ max}$ and J_{max} estimates were also similar across species, facilitating valid comparisons.

After each set of gas exchange measurements, needle length and width were measured, and the central angle of the needles was calculated (2π/# needles per fascicle) to estimate needle surface area in the chamber by assuming that needle cross section represents a circle sector. To test the approach, we measured both needle width and needle circumference from cross sections (four needles per tree and five trees per species) and calculated the ratio of circle sector-based estimate circumference ($C_{circle\ sector}$) to measured circumference (C). For comparison, we also calculated circumference assuming a pie-shaped cross section (C_{pie}; Niinemets, Ellsworth, Lukjanova, & Tobias, 2002) and the ratio of C_{pie} to C. The sampled fascicles were then oven dried to a constant mass at 65°C (for 48 hr), weighed and ground to determine foliage nitrogen (N) concentration with a Carlo-Erba analyser (Model NA 1500, Fison Instruments, Danvers, MA; USDA Forest Service Laboratory, Research Triangle Park, NC). Nitrogen concentration was expressed on needle total surface area basis (N_{area}, g m^{-2}), on mesophyll cells surface area basis ($N_{mesophyll\text{-}surf.}$, g m^{-2}, calculated as $N_{area}/(S_{mesophyll\text{-}surf.}/S_{needle})$), and on mass basis ($N_{mass}$, %). A and $V_{c,\ max}$ were expressed both on total area basis (A_{area}, $V_{c,\ max\text{-}area}$) and on mass basis (A_{mass}, $V_{c,\ max\text{-}mass}$), which were calculated as $A_{area}/LMA_{total\text{-}surf.}$ and $V_{c,\ max\text{-}area}/LMA_{total\text{-}surf}$. Stomatal conductance was expressed on total needle surface area basis.

2.5 | Statistical analysis

Individual trees were used as replicates. The effect of species on leaf anatomical, mechanical, chemical, and hydraulic traits were tested using one-way analysis of variance and the effect of species on g_s was tested by analysis of covariance incorporating the natural logarithm of leaf-to-air water vapour pressure deficit (VPD) as a covariate. Fisher's least significant difference test was used to identify the differences in those leaf traits among tree species. Linear regressions were used to evaluate relationships between leaf functional traits and needle length, and among leaf traits, across species. Probability levels $P < 0.05$ and $P < 0.10$ were considered to indicate a significant relationship and a tendency, respectively.

Leaf hydraulic traits and gas exchange were measured on separate campaigns, in 2015 and 2017, respectively. The laboratory measurements of leaf hydraulics represent optimal conditions at full saturation (and thus maximum K_{leaf}), and therefore, the means of g_s and A_{area} by species estimated in April (and under close to saturated soil moisture conditions) were used to analyse their potential relationships with the respective species-specific K_{leaf}. Because the measured g_s appeared sensitive to changes of VPD, the mean g_s and A_{area} of all the species were normalized to VPD at 1.5 KPa, which represents the mean VPD over all the measurements. Statistical analyses were performed using the SPSS software (version 19.0, SPSS, Inc., Cary, NC), and curve fits were performed using SigmaPlot (version 12.5, Systat Software, Inc., San Rafael, CA).

3 | RESULTS

3.1 | Variation in anatomical and morphological characteristics with needle length

Across species, needle length ranged from 7.5 ± 0.3 cm in *P. virginiana* to 34.6 ± 1.3 cm in *P. palustris*. In needle cross sections, the phloem area remained constant at ~2.1% over the range of needle lengths

TABLE 1 Needle morphological characteristics in five *Pinus* species (mean ± *SE*)

Needle morphological characteristics	*Pinus virginiana* (PV)	*Pinus echinata* (PEC)	*Pinus taeda* (PT2)	*Pinus taeda* (PT1)	*Pinus elliottii* (PEL)	*Pinus palustris* (PP)	*P* value
Needle length (cm)	7.51 ± 0.35^{d}	9.28 ± 0.57^{d}	17.32 ± 0.52^{c}	19.69 ± 0.41^{c}	23.23 ± 1.37^{b}	34.59 ± 1.31^{a}	0.0001
Width (mm)	1.69 ± 0.03^{a}	1.48 ± 0.02^{be}	1.41 ± 0.04^{de}	1.50 ± 0.04^{be}	1.58 ± 0.03^{bc}	1.61 ± 0.03^{ac}	0.0001
Thickness (mm)	0.78 ± 0.03^{a}	0.74 ± 0.02^{a}	0.62 ± 0.02^{b}	0.63 ± 0.02^{b}	0.76 ± 0.02^{a}	0.80 ± 0.02^{a}	0.0001
Cross-sectional area (mm^2)	1.01 ± 0.05^{a}	0.76 ± 0.05^{b}	0.59 ± 0.03^{d}	0.64 ± 0.03^{d}	0.90 ± 0.04^{ac}	0.86 ± 0.03^{bc}	0.0001
Circumference (mm)	4.15 ± 0.08^{a}	3.55 ± 0.08^{cd}	3.27 ± 0.09^{ef}	3.44 ± 0.08^{cf}	3.89 ± 0.09^{b}	3.76 ± 0.07^{bd}	0.0001
$LMA_{total\text{-}surf.}$ (g m^{-2})	98.87 ± 2.50^{a}	80.78 ± 4.11^{b}	81.49 ± 5.14^{b}	83.52 ± 1.60^{BC}	91.96 ± 3.75^{ac}	82.94 ± 1.64^{bc}	0.005
Dry/fresh mass (%)	37.57 ± 0.69^{a}	32.58 ± 0.77^{d}	36.72 ± 0.38^{ac}	37.05 ± 0.29^{a}	38.39 ± 0.64^{a}	35.22 ± 0.63^{bc}	0.0001

Note. Different lower case letters indicate significant differences ($P < 0.05$) in needle morphological characteristics among species according to Fisher's least significant difference test. LMA: leaf mass per area.

(Figures 2 and S1a), and the fractions of xylem, vascular bundle, transfusion tissue, central cylinder, and epidermal tissue increased with needle length (Figures 2 and S1b–f). Although the xylem comprised a small fraction (2.2 ± 0.1% to 4.5 ± 0.2%) of the cross-sectional area, it showed the largest relative increase of 108% with needle length, followed by the vascular bundle area, increasing 71%, from 3.9 ± 0.2% to 6.7 ± 0.2%. By contrast, the mesophyll tissue, which occupied the largest fraction (52.2 ± 0.9% to 64.3 ± 0.9%) of the cross-sectional area, decreased with increasing needle length by 23% (Figures 2 and S1g).

The decrease of mesophyll tissue cross-sectional area with needle length was associated with a tendency for increasing mesophyll cell size (Figure 3a). In addition, the mesophyll thickness was greater for the two species with the shortest needles compared with the other species except *P. elliottii* (maximum $P = 0.003$; Figure 3b). The combined effect of these responses was a decrease in total mesophyll surface area per leaf area ($S_{mesophyll\text{-}surf.}/S_{needle}$) with needle length (Figure 3c). Leaf morphological attributes (width, thickness, and circumference; Table 1) including needle cross-sectional area (Figure 4a) were insensitive to needle length, consistent with published data (Figure 1b, Table S1). Leaf mass per area ($LMA_{total\text{-}surf.}$), which reflects differences in both thickness and density among needles, was unrelated to needle length ($R^2 = 0.40$, $P = 0.17$). However, the fraction of mechanical or supporting tissue (epidermal tissue plus xylem) increased 35% from the shortest to the longest needles (Figure 4b), whereas both fresh and dry densities decreased 25% and 21%, respectively (Figure 4c). Both xylem tracheid diameter and hydraulic diameter increased ~27% across the range in needle length (Figure 4d). Taken together, the longer the needle, the larger was the fraction of its cross-sectional area made of xylem tissue containing larger tracheids. The increase in the supporting tissue (seen Figure 4b) is attributable to the increasing fraction of both the epidermal tissue and the xylem (Figure 5a). Furthermore, the fraction of mesophyll tissue was inversely related to that of mechanical tissue (Figure 5b), indicating a trade-off between assimilative and support tissues.

3.2 | Variation in needle hydraulics, gas exchange, and *N* with needle length

The ratio of circle sector-based estimate of circumference to measured circumference ($C_{circle\ sector}/C$) of only the two *P. taeda* families was significantly different from 1 (one-sample *t* test, $P < 0.05$). The deviation, however, was small (up to 4%; Table S2), and the regression between circle sector-based circumference and measured circumference across species was not different from the 1:1 line (Figure S2). Thus, the circle sector seems to represent the needle cross section of these species reasonably well, and using this simplified approximation was unlikely to affect the interpretation of the results.

Leaf hydraulic conductance (K_{leaf}) was positively correlated with needle length (Figure 6a), increasing from 0.46 ± 0.13 to 2.39 ± 0.35 mmol m^{-2} s^{-1} MPa^{-1}, or by 418% from the shortest to the longest needles. Moreover, one component of K_{leaf}, the xylem hydraulic conductance (K_{xylem}), increased with needle length across

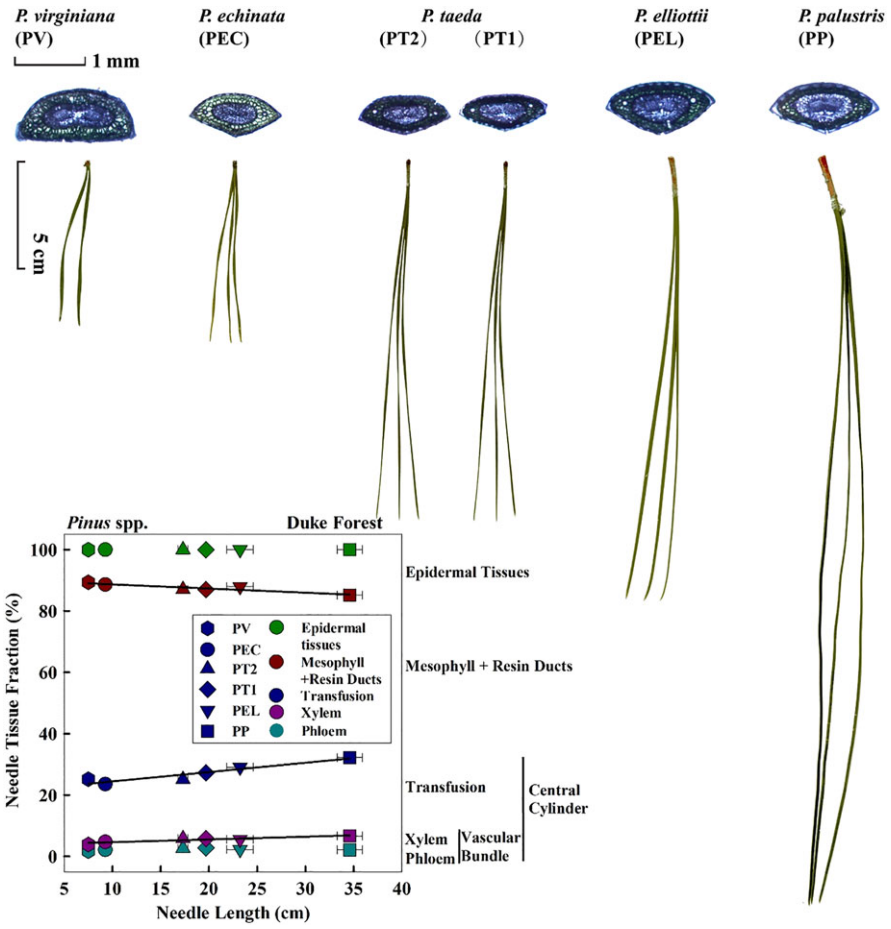

FIGURE 2 Needle cross sections, leaf size, and the relationships between needle length and fractions of various needle tissues in five *Pinus* species (maximum $P = 0.01$). Symbols represent species mean values ($n = 5$) and error bars represent standard error

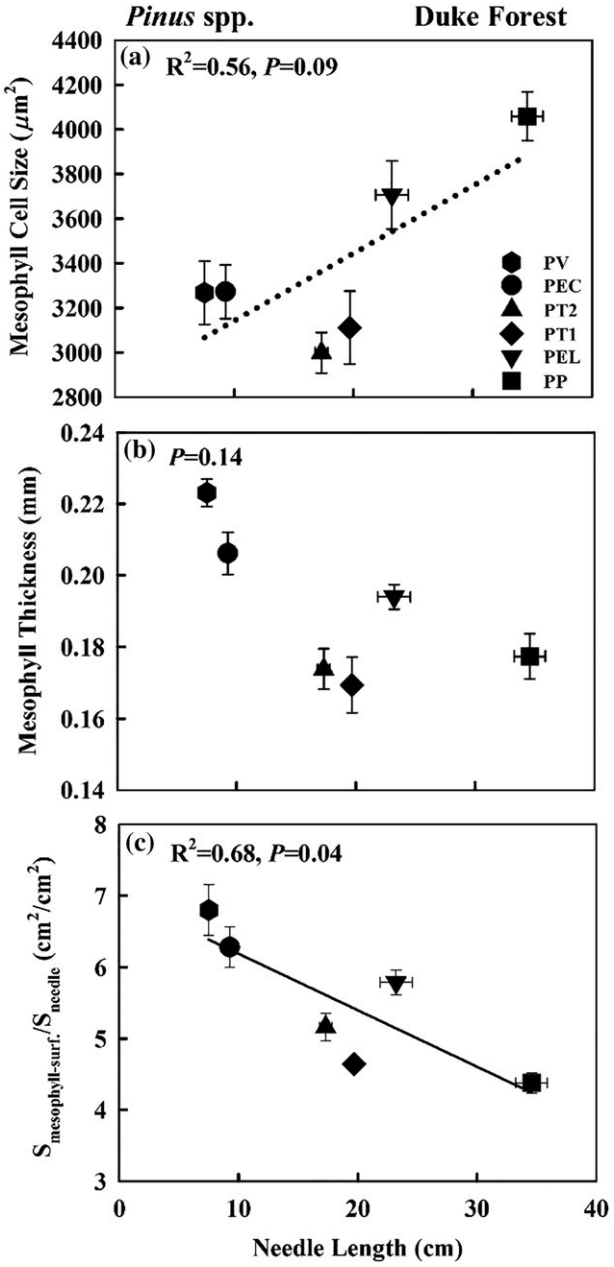

FIGURE 3 Variation in mesophyll cell size (a), mesophyll thickness (b), and mesophyll cells surface area per needle surface area ($S_{mesophyll\text{-}surf.}/S_{needle}$; c) with needle length in five *Pinus* species. Symbols represent species means (n = 5), and error bars represent standard error. Solid and dotted lines represent regressions with $P < 0.05$ and $P < 0.10$, respectively. PV: *Pinus virginiana*; PEC: *Pinus echinata*; PT2 and PT1: *Pinus taeda*; PEL: *Pinus elliottii*; PP: *Pinus palustris*

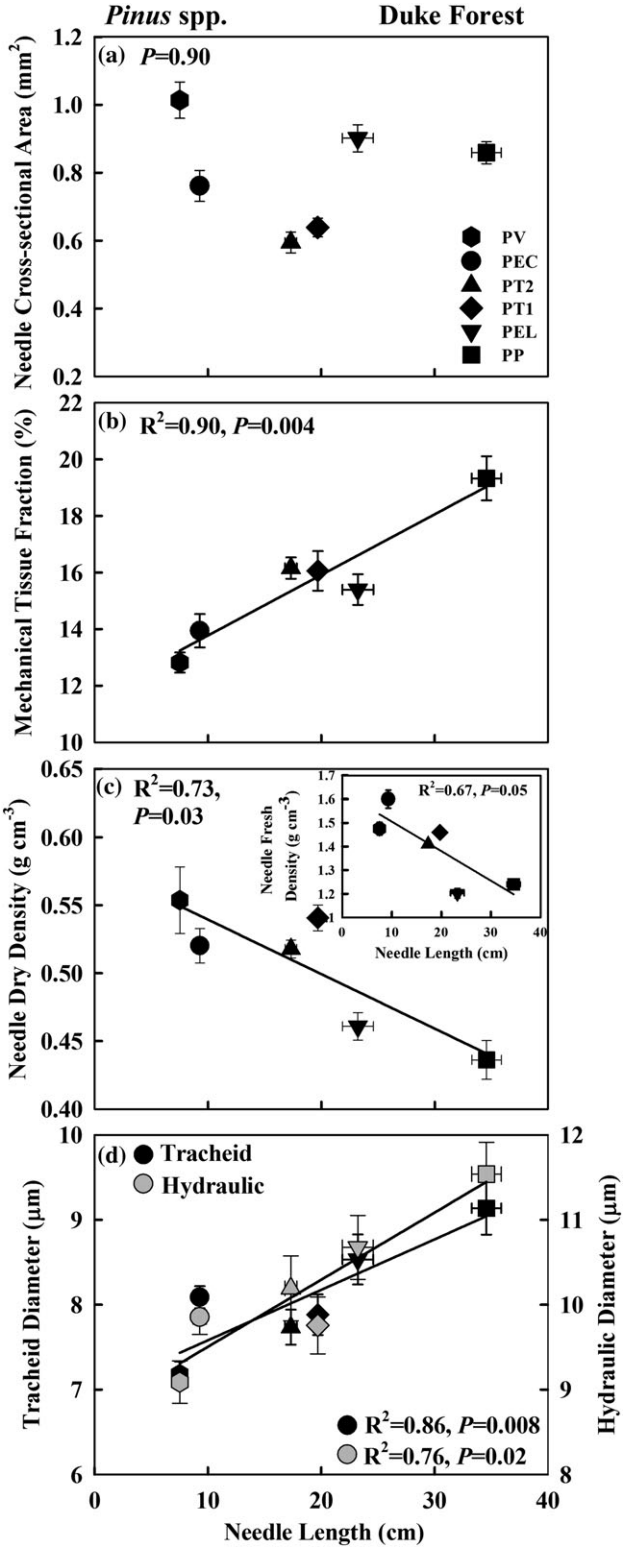

FIGURE 4 Variation in needle mechanical, morphological, and anatomical characteristics with needle length in five *Pinus* species. (a) Needle cross-sectional area, (b) mechanical tissue fraction, (c) dry (and fresh) density, and (d) tracheid diameter and hydraulic diameter. Symbols represent species means (n = 5), and error bars represent standard error. PV: *Pinus virginiana*; PEC: *Pinus echinata*; PT2 and PT1: *Pinus taeda*; PEL: *Pinus elliottii*; PP: *Pinus palustris*

species by 420% (Figure 6b), with the variation in K_{xylem} explaining 83% of that in K_{leaf} across species (Figure 6c).

We found a strong relationship between the light-saturated photosynthetic rate per unit needle surface area (A_{area}) and stomatal conductance (g_s) *within* species (Figure S3a). g_s and intercellular-to-ambient (CO_2) ratio (C_i/C_a) declined with increasing leaf-to-air water VPD for most species (Figure S3b,c). Positive relation between A_{area} and g_s was also observed *among* species (Figure 7a). However, it should be noted that, compared with hydraulic properties, the range of variation among species in all gas exchange-based variables was

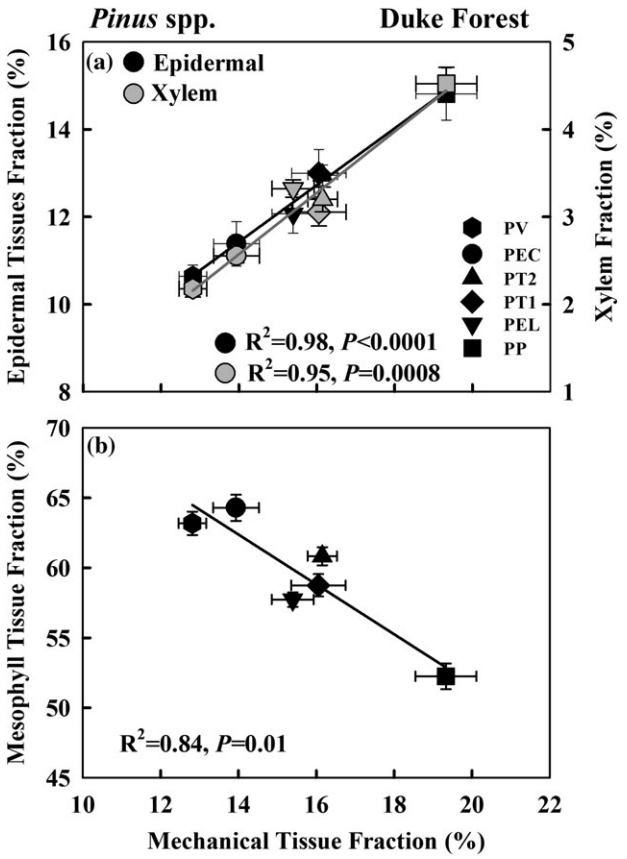

FIGURE 5 Variation in needle anatomical traits with mechanical tissue fraction in five *Pinus* species. (a) Epidermal tissues fraction and xylem fraction, and (b) mesophyll tissue fraction. Symbols represent species means (n = 5), and error bars represent standard error. PV: *Pinus virginiana*; PEC: *Pinus echinata*; PT2 and PT1: *Pinus taeda*; PEL: *Pinus elliottii*; PP: *Pinus palustris*

substantially smaller. *P. palustris* with the longest needles showed the highest g_s (110 ± 28 mmol m^{-2} s^{-1}) and A_{area} (7.2 ± 0.6 μmol m^{-2} s^{-1}), whereas *P. echinata* had the lowest g_s (79 ± 17 mmol m^{-2} s^{-1}) and A_{area} (6.1 ± 0.6 μmol m^{-2} s^{-1}). Across all species, C_i/C_a showed no trend with needle length (Figure 7b), whereas g_s tended to increase with needle length driving a similar trend in A_{area} (Figure 7c). Consequently, A_{area} showed a tendency to increase with K_{leaf} (Figure 7d). Light-saturated photosynthetic rate per unit mass (A_{mass}) showed no trend with needle length across species (Figure S4a).

Although A_{area} tended to increase with needle length across species, maximum carboxylation capacity on area basis ($V_{c,\ max\text{-}area}$) and on mass basis ($V_{c,\ max\text{-}mass}$) did not. Thus, the observed variation in light-saturated photosynthetic rate was unrelated to the maximum rates of carboxylation. Furthermore, N content on needle surface area basis (N_{area}) decreased with needle length (Figure 8a) with an estimated maximum N_{area} of 1.02 ± 0.08 g m^{-2} for *P. echinata* and a minimum of 0.69 ± 0.04 g m^{-2} for *P. palustris*. Hence, A_{area} was inversely correlated with N_{area} (Figure 8b), and the variation in $V_{c,max\text{-}area}$ was unrelated to N_{area} (Figure 8c). N content on mesophyll cell surface area basis ($N_{mesophyll\text{-}surf}$) was insensitive to needle length (Figure S4b, R^2 = 0.04, P = 0.70). Nitrogen concentration (N_{mass}) showed no trend with needle length (Figure 8d) and did not explain the variation in either A_{mass} or $V_{c,\ max\text{-}mass}$ (Figure 8e,f). The decrease in N_{area} with increasing needle length was attributable to a decrease in the fraction of mesophyll tissue (Figure 9). Summarizing, although mesophyll tissue fraction and N_{area} decreased with increasing needle length, C_i/C_a and $V_{c,max\text{-}area}$ were unresponsive, and g_s and A_{area} tended to increase.

4 | DISCUSSION

Our results demonstrate that needle anatomy varies with needle length among the five pine species studied (Figures 2 and S1). The anatomical differences reflected adjustments in the capacity for mechanical support and leaf hydraulic conductance (K_{leaf}) as needles increased in length, suggesting coordination among leaf traits. With increasing needle length, the fraction of mechanical tissue increased, whereas tissue density decreased (Figure 4). The increase of K_{leaf} was likely related to larger mean hydraulic diameter (Figure 4d) and shorter pathway for water movement through the mesophyll (Figure 3; Scoffoni et al., 2016). Changes in these trait values were, in turn, accompanied with similar (in direction) changes in gas exchange characteristics, such as stomatal conductance (g_s) and light-saturated photosynthetic rate per unit leaf area (A_{area}; Figure 7).

4.1 | Needle length and traits related to mechanical support

Following our first hypothesis (H1a), we show that mechanical tissue volume fraction increases with needle length (Figure 4b), consistent with the increased requirements for support, as the bending moment operating on a needle increases with length (Gere & Timoshenko, 1997; Niklas, 1992, 1999). Moreover, similar to the findings on volume fractions in three Mediterranean pines (Kuusk, Niinemets, & Valladares, 2018a), we found a trade-off between the relative fractions of support versus photosynthetic tissue (mesophyll) across species (Figure 5b). Our results suggest that increasing structural stiffness comes at the cost of tissues involved in photosynthesis, in both relative and absolute terms because the cross-sectional area did not increase with needle length (Figure 4a). Our results add to the previous findings on positive relation between leaf size and investment to supporting tissues (Givnish, 1984; Niinemets, Portsmuth, & Tobias, 2006; Niinemets & Sack, 2006). They suggest that leaf size, here determined primarily by needle length, strongly influences anatomical traits and that redistribution from photosynthetic to mechanical tissues as needles grow longer may be necessary to maintain surface exposure to incoming light.

Among the supporting tissues, the xylem fraction (of the needle cross section) was found most sensitive to changes in needle length. Increases in leaf size would inevitably require increased support and transpiration requirements at the leaf scale. Our results suggest that, although there may be a trade-off between investments in light harvesting (i.e., interception of incoming radiation supported by mechanical tissue), versus carbon fixation (photosynthesis tissue), the trade-off is less costly for photosynthesis than it may appear for two reasons. First, investing more in xylem is an investment in both the mechanical tissue facilitating light capture (by reducing needle bending

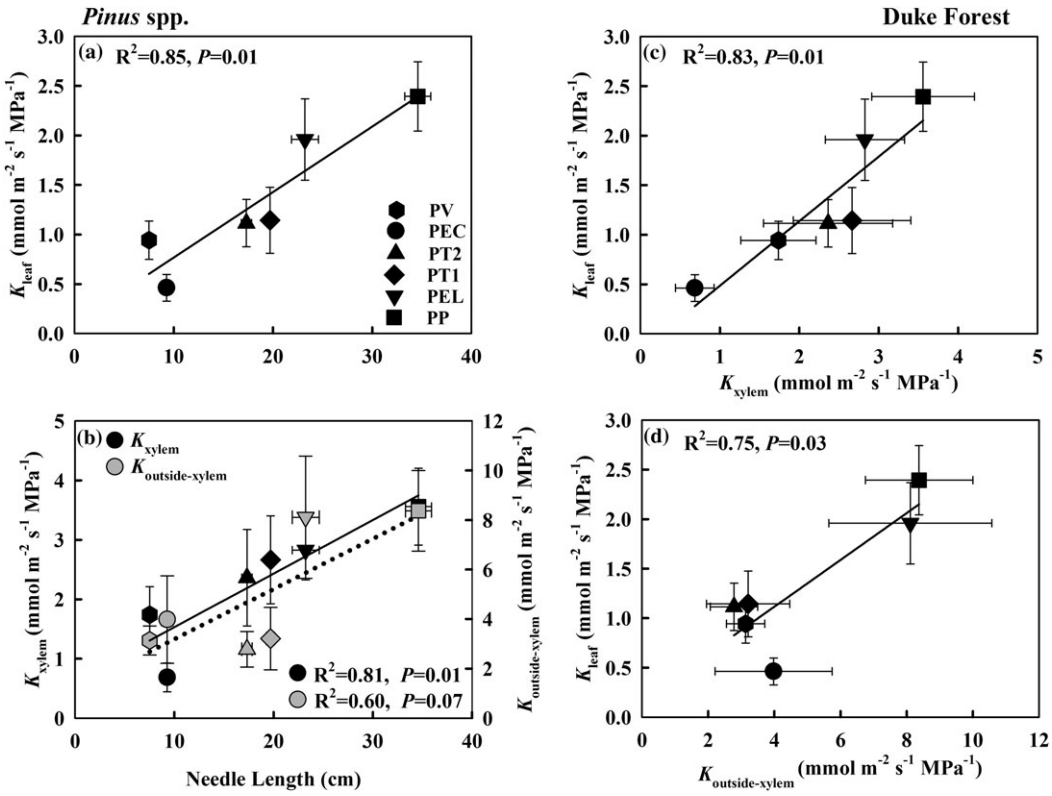

FIGURE 6 Variation in needle hydraulic properties in five *Pinus* species. Leaf hydraulic conductance (K_{leaf}; a), xylem hydraulic conductance (K_{xylem}) and outside-xylem hydraulic conductance ($K_{outside\text{-}xylem}$; b) as a function of needle length, and K_{leaf} as a function of K_{xylem} (c) and $K_{outside\text{-}xylem}$ (d). Symbols represent species means (n = 5), and error bars represent standard error. Solid and dotted lines represent regressions with $P < 0.05$ and $P < 0.10$, respectively. PV: *Pinus virginiana*; PEC: *Pinus echinata*; PT2 and PT1: *Pinus taeda*; PEL: *Pinus elliottii*; PP: *Pinus palustris*

and self-shading) and the water transport system (by satisfying the greater demand for hydraulic conductivity), thereby reducing stomatal limitation to photosynthesis. Second, the properties of the tissues also changed with increasing needle length such that total needle volume density decreased (Figure 4c). As a result, the gravitational pull from its own weight per unit of length tended to decline (Figure S4c), reducing the mechanical force resulting from the increasing load applied along the needle. Thus, the increased investment in mechanical support is less than expected based on the change in length (Niklas, 1992), and conversely, the decrease in photosynthetic tissue was not as drastic as it might have been without adjustments to the properties of the tissues.

The changes in needle density seem related to anatomical adjustments. Because epidermis occupies only a small volume fraction and its density was shown to be low compared to other tissues (Poorter, Niinemets, Poorter, Wright, & Villar, 2009), we assumed that the effect of variation of epidermis fraction on volume density was negligible. Thus, the variation of density should be driven by changes in mesophyll and vascular tissue density and the shifts in their volume fractions. Individual mesophyll cell size tended to increase with increasing needle length (Figure 3a), suggesting that mesophyll tissue density tended to decrease with needle length. Furthermore, tracheid diameter also increased with needle length (Figure 4d), implying that the vascular tissue density decreased. Thus, although the vascular tissue density is higher than that of the mesophyll (Poorter et al., 2009) and vascular tissue fraction increased with needle length in our study, needle density decreased. The decrease in needle density with length reduced the rate of increase in mechanical support required to counter the gravity effect on needle display.

4.2 | Needle length and hydraulics

We found that K_{leaf} scaled with needle length across species (Figure 6 a), consistent with the increasing need for water transport (H1b). The differences observed in maximum K_{leaf} among species were associated with differences in xylem hydraulic conductance (K_{xylem}; Figure 6c), in agreement with the pattern observed in other tree species (Domec et al., 2016; Scoffoni et al., 2016). Xylem hydraulic conductance depends on both the tracheid lumen conductance (K_{lumen}) and the pit membrane conductance (K_{pits}; Domec et al., 2016; Pittermann, Sperry, Hacke, Wheeler, & Sikkema, 2006). Based on Hagen-Poiseuille's law, K_{lumen} scales with hydraulic diameter to the fourth power (Tyree & Ewers, 1991). Previous modelling studies have also shown that K_{xylem} increases with more and larger xylem conduits across species (Sack & Frole, 2006; Sommerville, Sack, & Ball, 2012). In our study, the increase in hydraulic diameter with needle length (Figure 4d) suggested that K_{lumen} increases with needle length. The outside-xylem hydraulic conductance ($K_{outside\text{-}xylem}$) showed a similar trend (Figure 6b). We found that mesophyll cell size tended to increase, yet the ratio of mesophyll cell surface area to needle surface area ($S_{mesophyll\text{-}surf.}/S_{needle}$) decreased with needle length (Figure 3), likely reducing the path length of water movement from the xylem

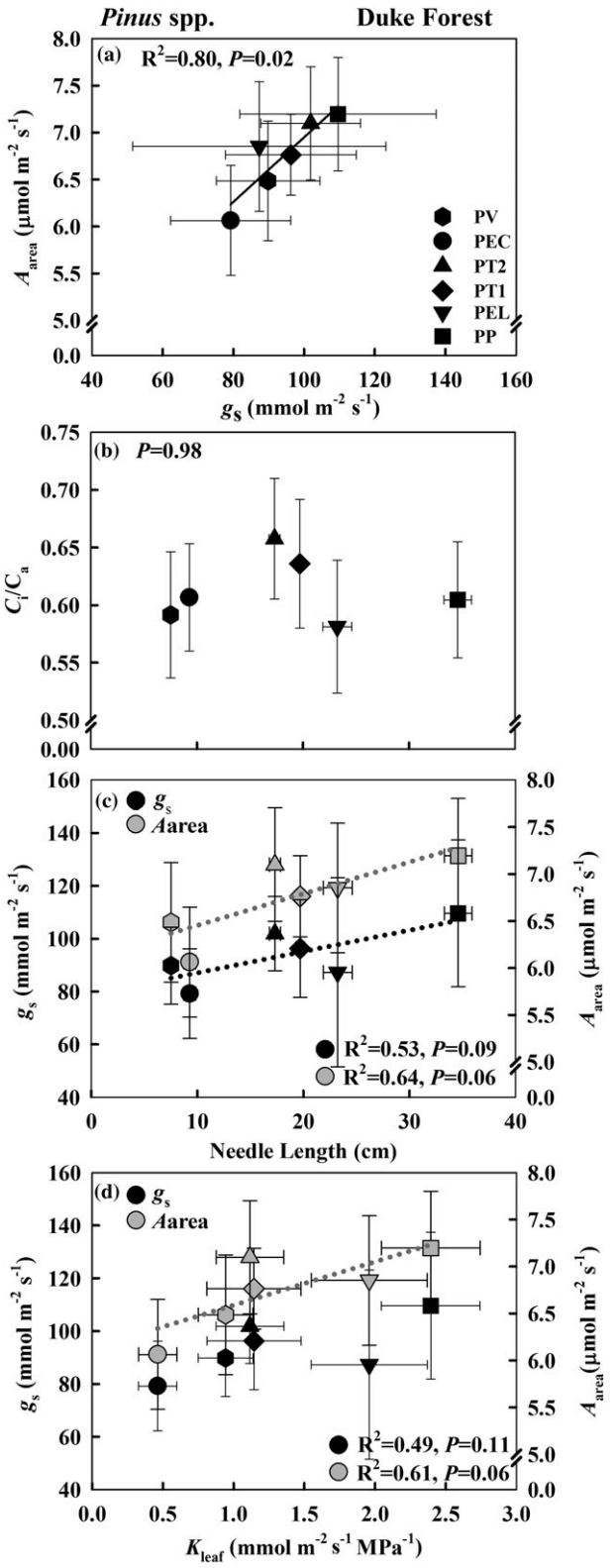

FIGURE 7 Relationships between (a) light-saturated photosynthetic rate on total needle surface area basis (A_{area}) and stomatal conductance (g_s), (b) intercellular to ambient CO_2 concentration ratio (C_i/C_a) and needle length, (c) g_s, A_{area} and needle length, and (d) g_s, A_{area} and leaf hydraulic conductance (K_{leaf}) in five *Pinus* species. Symbols represent species means (n = 10 for g_s and A_{area} and n = 5 for K_{leaf}), and error bars represent standard error. Solid and dotted lines represent regressions with $P < 0.05$ and $P < 0.10$, respectively. PV: *Pinus virginiana*; PEC: *Pinus echinata*; PT2 and PT1: *Pinus taeda*; PEL: *Pinus elliottii*; PP: *Pinus palustris*

across the mesophyll tissue to the stomata in longer needles, potentially explaining the increase in $K_{outside\text{-}xylem}$ (Brodribb et al., 2007).

It is noteworthy that the increase of $K_{outside\text{-}xylem}$ was not continuous with needle length, but our estimates for *P. elliottii* and *P. palustris* (two species with the longest needles) were much higher than the rest of the species or, alternatively, the estimates of $K_{outside\text{-}xylem}$ of both *P. taeda* families were lower than expected based on needle length. It is possible that in order to satisfy the increased transpiration requirements of long needles with large surface area, in addition to decreasing the path length of water movement within mesophyll tissue, other adjustments may be necessary to further increase $K_{outside\text{-}xylem}$. Based on previous studies, such strategies could include a combination of (a) increasing transfusion tissue fraction (Figure 2) to enhance radial water transport between the axial xylem and bundle sheath (Zhang, Rockwell, Wheeler, & Holbrook, 2014), and (b) improving the aquaporin activity and/or density, which increase the permeability of membranes (Chaumont & Tyerman, 2014; Maurel, 1997). Alternatively, it is possible that the smaller mesophyll cell size of *P. taeda* (Figure 3a), perhaps associated with other unmeasured changes, reduced $K_{outside\text{-}xylem}$ relative to that expected based on needle length, despite having a thinner mesophyll (Figure 3b). Future research in needle anatomical traits could focus on the role of the outside-xylem structure in determining $K_{outside\text{-}xylem}$.

4.3 | Needle length and gas exchange characteristics

Consistent with H1c, stomatal conductance (g_s) tended to increase with K_{leaf}, and needle length (Figure 7c,d), suggesting that among-species variation in needle anatomy and K_{leaf} may scale up to tree transpiration and leaf gas exchange (McCulloh et al., 2015; Sack & Holbrook, 2006). When stomata are open to allow diffusion of CO_2 into the leaf, water vapour is lost to the atmosphere, potentially dehydrating the leaf. The imbalance between the rate of evaporation and the rate of liquid water supply to the site of evaporation leads to substantial variation in leaf water potential, reflected in stomatal response designed to protect the xylem from cavitation (Oren et al., 1999; Sperry, Hacke, Oren, & Comstock, 2002). Thus, the capacity of plants to replace transpired water plays an important role in determining the stomatal conductance and associated photosynthetic rates. Indeed, because of that, A_{area} and g_s are highly correlated (Figure 7a; Damour, Simonneau, Cochard, & Urban, 2010; Wong, Cowan, & Farquhar, 1979), and because g_s is the gas-phase equivalent of K_{leaf}, it is not surprising that A_{area} tended to increase with K_{leaf} (Figure 7d). This finding is consistent with previous studies showing that A_{area} of leaves is often limited by the ability of the leaf hydraulic system to maintain leaves sufficiently hydrated for stomata to remain fully open (Brodribb, Holbrook, Zwieniecki, & Palma, 2005; Hao, Wheeler, Holbrook, & Goldstein, 2013). Therefore, increased K_{leaf} with needle length appears to exert the greatest influence on A_{area}.

The overwhelming control over A_{area} by needle-scale hydraulic properties refutes our final hypothesis (H2) that across the five pine species, A_{area} is also reflecting the prevailing light conditions on the needle surfaces as affected by differences in within-shoot mutual shading across species (Figure 1a; Niinemets, Tobias, et al., 2006;

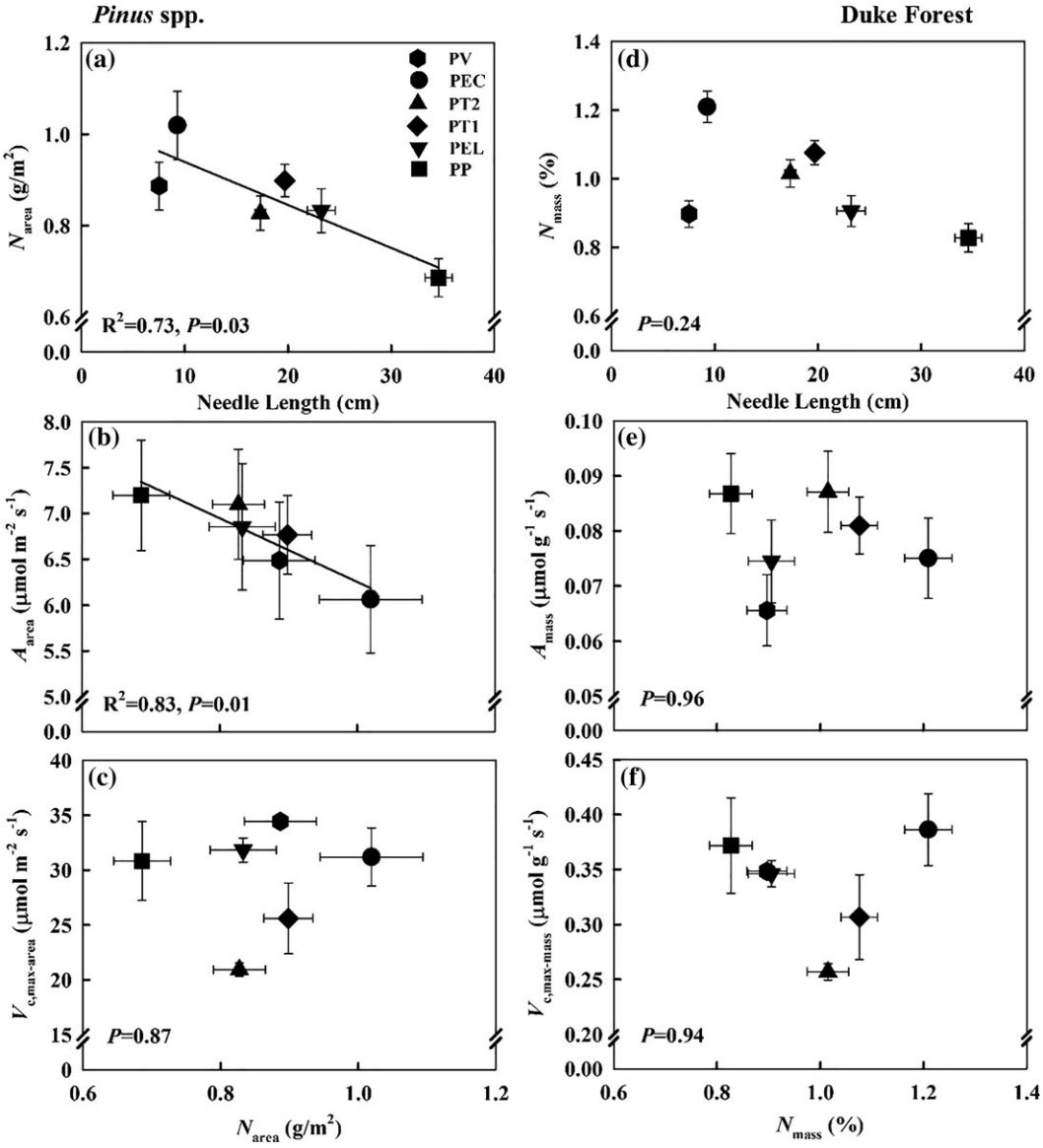

FIGURE 8 Variation in needle *N* content (total surface area; N_{area}) with needle length (a), and in area-based light-saturated photosynthetic rate (A_{area}) and maximum carboxylation capacity on total needle surface area basis ($V_{c,max\text{-}area}$) with N_{area} (b, c). Variation in needle *N* concentration (N_{mass}) with needle length (d), and in mass-based light-saturated photosynthetic rate (A_{mass}), and maximum carboxylation capacity ($V_{c,\ max\text{-}mass}$) with N_{mass} (e, f). Symbols represent species means (n = 5), and error bars represent standard error. PV: *Pinus virginiana*; PEC: *Pinus echinata*; PT2 and PT1: *Pinus taeda*; PEL: *Pinus elliottii*; PP: *Pinus palustris*

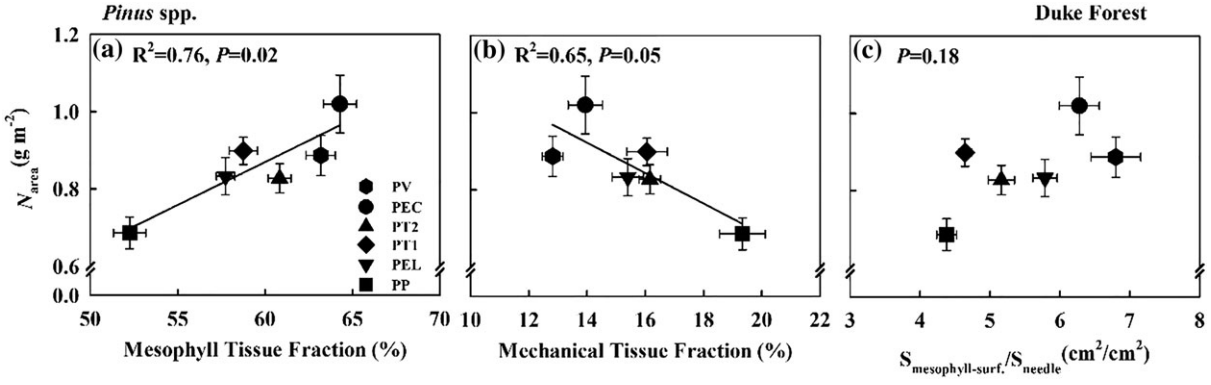

FIGURE 9 Variation in needle *N* content (total surface area; $N_{area.}$) with (a) mesophyll tissue fraction, (b) mechanical tissue fraction, and (c) mesophyll cell surface area per needle surface area ($S_{mesophyll\text{-}surf.}/S_{needle}$) in five *Pinus* species. Symbols represent species means (n = 5), and error bars represent standard error. PV: *Pinus virginiana*; PEC: *Pinus echinata*; PT2 and PT1: *Pinus taeda*; PEL: *Pinus elliottii*; PP: *Pinus palustris*

Stenberg et al., 1994; Thérézien et al., 2007). Such effect has been shown numerous times *within species* in response to growing-light environment and within-canopy light gradients, in both conifers and broadleaved species (e.g., Niinemets, Keenan, & Hallik, 2015; Niinemets, Lukjanova, Turnbull, & Sparrow, 2007; Oren, Schulze, Matyssek, & Zimmermann, 1986; Stenberg et al., 2001), presumably due to changes in leaf thickness, mesophyll fraction, and mesophyll-cell-to-needle-surface-area ratio ($S_{\text{mesophyll-surf.}}/S_{\text{needle}}$; Nobel et al., 1975). Here, however, differences among species in the interception efficiency may be too small for the presumed effects on photosynthetic capacity to clearly manifest. This is especially so considering that the two hypothesized responses (light-driven and hydraulics-driven) would produce similar effect on photosynthesis of increasing with needle length at the low-mid portion of the range, with diverging effects noticeable only at the higher end. Summarizing, across species, positive trends in K_{leaf}, g_s, and A_{area} with needle length conflicted with an inverse linear relation in $S_{\text{mesophyll-surf.}}/S_{\text{needle}}$ (Figure 3c), suggesting that the hydraulic control over photosynthetic rate dominated over other leaf-scale controls of photosynthetic capacity.

Indeed, in addition to inverse patterns of A_{area} and $S_{\text{mesophyll-surf.}}/S_{\text{needle}}$ with needle length, both area-based and mass-based estimates of needle photosynthetic capacity across the pines were poorly related (or inversely related) to indicators of biochemical capacity. Maximum carboxylation capacity ($V_{c,\ max}$), whether expressed on mass or area basis, showed no trend with needle length and was unrelated to variation in foliar *N* (Figure 8c,f). Variations in A_{mass} were not reflecting those in foliar *N* concentration (Figure 8e). The decrease in N_{area} with increasing needle length (Figure 8a) generated an inverse relationship between A_{area} and N_{area} (Figure 8b), which further suggests that photosynthetic nitrogen use efficiency (*A*/*N*) increased with needle length. The tendency of A_{area} to increase with needle length was mainly driven by a similar tendency in g_s (Figure 7), although the decrease in N_{area} with needle length likely reflected the redistribution of tissue between mesophyll and mechanical support (Figure 9), suggested by the insensitivity of $N_{\text{mesophyll-surf}}$ to needle length (Figure S4b). In other words, it seems that the photosynthetic apparatus was of sufficient amount to respond to g_s across species, such that increasing conductance with needle length resulted in increasing photosynthetic rate, keeping C_i/C_a relatively similar. The decoupling between A_{mass} and N_{mass} is inconsistent with the world-wide "leaf economic spectrum" (Wright et al., 2004) yet in line with other studies on conifers failing to detect a positive relation between A_{mass} and N_{mass} (Bauer et al., 2004; Kuusk et al., 2018b). In our dataset, this might be due to the narrow range in N_{mass} among species, which occupy the low return end of the leaf economics spectrum. Furthermore, we analysed needles for total foliar *N*, although it is known that there is broad flexibility in the partitioning of *N* among photosynthetic and non-photosynthetic functions across species (Onoda et al., 2017). For example, a significant and potentially species-specific fraction of foliar *N* may be invested in protective chemicals (Kursar & Coley, 2003; Levin, 1976). Among the species in this study, the short needles of *P. virginiana* and *P. echinata* have a longer lifespan (2–5 years vs. <2 years for the other three species; Ewers & Schmid, 1981), potentially requiring greater investment in protective chemicals. Taken together, our study suggested that the correlations of leaf functional traits in conifers might deviate from the universal relationships, which potentially indicate multiple drivers of leaf trait variation at different taxonomic scales (Anderegg et al., 2018; Osnas et al., 2018).

As a final note, we wish to point out that, in this study, g_s and *A* were estimated at the leaf scale, although the actual consequences of various structural designs on carbon gain and water use must ultimately be evaluated at scales from shoots (the functional unit) to crowns and canopies. An ongoing work is aimed at measuring and scaling hydraulic traits to match the modelled mean light environment and to assess whether these up-scaled photosynthetic and hydraulic capacities (or rates) are coordinated, thus matching mean stomatal conductance with mean light availability.

ACKNOWLEDGEMENTS

N.W. gratefully acknowledges the financial support from the China Scholarship Council for the study abroad at Duke University. Financial support for R.O. was provided by the Erkko Visiting Professor Programme of the Jane and Aatos Erkko 375th Anniversary Fund, through the University of Helsinki. This research was also partially supported by a grant from the National Science Foundation (NSF-IOS-1754893). We thank Juan Chen and Yizheng Wang for their help in the field and the NC State University Cooperative Tree Improvement Program and the USDA Forest Service for access to the Longleaf Pine Regional Provenance/Progeny Trial in the Duke Forest.

ORCID

Na Wang https://orcid.org/0000-0002-3063-1706
Sari Palmroth https://orcid.org/0000-0002-1290-4280
Jean-Christophe Domec https://orcid.org/0000-0003-0478-2559
Ram Oren https://orcid.org/0000-0002-5654-1733

REFERENCES

Anderegg, L. D., Berner, L. T., Badgley, G., Sethi, M. L., Law, B. E., & HilleRisLambers, J. (2018). Within-species patterns challenge our understanding of the leaf economics spectrum. *Ecology Letters*, *21*(5), 734–744. https://doi.org/10.1111/ele.12945

Bauer, G., Bazzaz, F., Minocha, R., Long, S., Magill, A., Aber, J., & Berntson, G. (2004). Effects of chronic *N* additions on tissue chemistry, photosynthetic capacity, and carbon sequestration potential of a red pine (*Pinus resinosa* Ait.) stand in the NE United States. *Forest Ecology and Management*, *196*, 173–186. https://doi.org/10.1016/j.foreco.2004.03.032

Bernacchi, C. J., Singsaas, E. L., Pimentel, C., Portis, A. R. Jr., & Long, S. P. (2001). Improved temperature response functions for models of Rubisco-limited photosynthesis. *Plant, Cell and Environment*, *24*, 253–260. https://doi.org/10.1111/j.1365-3040.2001.00668.x

Booker, R. E. (1977). Problems in the measurement of longitudinal sapwood permeability and hydraulic conductivity. *N.Z. Journal of Forest Science*, *7*, 297–306.

Brodribb, T. J., Feild, T. S., & Jordan, G. J. (2007). Leaf maximum photosynthetic rate and venation are linked by hydraulics. *Plant Physiology*, *144*, 1890–1898. https://doi.org/10.1104/pp.107.101352

Brodribb, T. J., Holbrook, N. M., Zwieniecki, M. A., & Palma, B. (2005). Leaf hydraulic capacity in ferns, conifers and angiosperms: Impacts on photosynthetic maxima. *New Phytologist*, *165*, 839–846. https://doi.org/10.1111/j.1469-8137.2004.01259.x

Chaumont, F., & Tyerman, S. D. (2014). Aquaporins: Highly regulated channels controlling plant water relations. *Plant Physiology*, *164*, 1600–1618. https://doi.org/10.1104/pp.113.233791

Cochard, H., Froux, F., Mayr, S., & Coutand, C. (2004). Xylem wall collapse in water-stressed pine needles. *Plant Physiology*, *134*, 401–406. https://doi.org/10.1104/pp.103.028357

Corner, E. J. H. (1949). The durian theory or the origin of the modern tree. *Annals of Botany*, *13*, 367–414. https://doi.org/10.1093/oxfordjournals.aob.a083225

Damour, G., Simonneau, T., Cochard, H., & Urban, L. (2010). An overview of models of stomatal conductance at the leaf level. *Plant, Cell and Environment*, *33*, 1419–1438.

Domec, J., Palmroth, S., Ward, E., Maier, C., Thereuzien, M., & Oren, R. (2009). Interactive effects of long term elevated CO_2 and N-fertilization on the coordination between lead hydraulic conductance and stomatal conductance in *Pinus taeda*. *Plant, Cell and Environment*, *32*, 1500–1512. https://doi.org/10.1111/j.1365-3040.2009.02014.x

Domec, J.-C., Palmroth, S., & Oren, R. (2016). Effects of *Pinus taeda* leaf anatomy on vascular and extravascular leaf hydraulic conductance as influenced by N-fertilization and elevated CO_2. *Journal of Plant Hydraulics*, *3*, e007.

Esau, K. (1977). *Anatomy of seed plants* (2nd ed.). New York, USA: John Wiley & Sons.

Ewers, F. W., & Schmid, R. (1981). Longevity of needle fascicles of *Pinus longaeva* (bristlecone pine) and other North American pines. *Oecologia*, *51*, 107–115. https://doi.org/10.1007/BF00344660

Falster, D. S., & Westoby, M. (2003). Leaf size and angle vary widely across species: What consequences for light interception? *New Phytologist*, *158*, 509–525. https://doi.org/10.1046/j.1469-8137.2003.00765.x

Farquhar, G. V., von Caemmerer, S. V., & Berry, J. (1980). A biochemical model of photosynthetic CO_2 assimilation in leaves of C_3 species. *Planta*, *149*, 78–90. https://doi.org/10.1007/BF00386231

Gere, J., & Timoshenko, S. (1997). *Mechanics of materials* (4th ed.). Boston, MA, USA: PWS Publishing Co.

Givnish, T. J. (1984). Leaf and canopy adaptations in tropical trees. In E. Medina, H. A. Mooney, & C. Vazquez-Yanes (Eds.), *Physiological ecology of plants of the wet tropics* (pp. 51–84). The Hague, The Netherlands: Dr W. Junk.

Hao, G.-Y., Wheeler, J. K., Holbrook, N. M., & Goldstein, G. (2013). Investigating xylem embolism formation, refilling and water storage in tree trunks using frequency domain reflectometry. *Journal of Experimental Botany*, *64*, 2321–2332. https://doi.org/10.1093/jxb/ert090

Johnson, J. D. (1984). A rapid technique for estimating total surface area of pine needles. *Forest Science*, *30*, 913–921.

Kolb, K., & Sperry, J. (1999). Transport constraints on water use by the Great Basin shrub, Artemisia tridentata. *Plant, Cell and Environment*, *22*, 925–936. https://doi.org/10.1046/j.1365-3040.1999.00458.x

Koralewski, T. E., Mateos, M., & Krutovsky, K. V. (2016). Conflicting genomic signals affect phylogenetic inference in four species of North American pines. *Aob Plants*, *8*, plw019.

Kursar, T. A., & Coley, P. D. (2003). Convergence in defense syndromes of young leaves in tropical rainforests. *Biochemical Systematics and Ecology*, *31*, 929–949. https://doi.org/10.1016/S0305-1978(03)00087-5

Kuusk, V., Niinemets, Ü., & Valladares, F. (2018a). A major trade-off between structural and photosynthetic investments operative across plant and needle ages in three Mediterranean pines. *Tree Physiology*, *38*, 543–557. https://doi.org/10.1093/treephys/tpx139

Kuusk, V., Niinemets, Ü., & Valladares, F. (2018b). Structural controls on photosynthetic capacity through juvenile-to-adult transition and needle ageing in Mediterranean pines. *Functional Ecology*, *32*, 1479–1491. https://doi.org/10.1111/1365-2435.13087

Levin, D. A. (1976). The chemical defenses of plants to pathogens and herbivores. *Annual Review of Ecology and Systematics*, *7*, 121–159. https://doi.org/10.1146/annurev.es.07.110176.001005

Maurel, C. (1997). Aquaporins and water permeability of plant membranes. *Annual Review of Plant Physiology and Plant Molecular Biology*, *48*, 399–429. https://doi.org/10.1146/annurev.arplant.48.1.399

McCulloh, K. A., Johnson, D. M., Petitmermet, J., McNellis, B., Meinzer, F. C., & Lachenbruch, B. (2015). A comparison of hydraulic architecture in three similarly sized woody species differing in their maximum potential height. *Tree Physiology*, *35*, 723–731. https://doi.org/10.1093/treephys/tpv035

Medlyn, B., Dreyer, E., Ellsworth, D., Forstreuter, M., Harley, P., Kirschbaum, M., … Walcroft, A. (2002). Temperature response of parameters of a biochemically based model of photosynthesis. II. A review of experimental data. *Plant, Cell and Environment*, *25*, 1167–1179. https://doi.org/10.1046/j.1365-3040.2002.00891.x

Melcher, P. J., Holbrook, M. N., Burns, M. J., Zwieniecki, M. A., Cobb, A. R., Brodribb, T. J., … Sack, L. (2012). Measurements of stem xylem hydraulic conductivity in the laboratory and field. *Methods in Ecology and Evolution*, *3*, 685–694. https://doi.org/10.1111/j.2041-210X.2012.00204.x

Milla, R., & Reich, P. B. (2007). The scaling of leaf area and mass: The cost of light interception increases with leaf size. *Proceedings of the Royal Society B: Biological Sciences*, *274*, 2109–2114.

Nardini, A., & Salleo, S. (2000). Limitation of stomatal conductance by hydraulic traits: Sensing or preventing xylem cavitation? *Trees-Structure and Function*, *15*, 14–24. https://doi.org/10.1007/s004680000071

Nardini, A., Salleo, S., & Raimondo, F. (2003). Changes in leaf hydraulic conductance correlate with leaf vein embolism in *Cercis siliquastrum* L. *Trees Structure and Function*, *17*, 529–534. https://doi.org/10.1007/s00468-003-0265-z

Niinemets, Ü., Ellsworth, D. S., Lukjanova, A., & Tobias, M. (2002). Dependence of needle architecture and chemical composition on canopy light availability in three North American *Pinus* species with contrasting needle length. *Tree Physiology*, *22*, 747–761. https://doi.org/10.1093/treephys/22.11.747

Niinemets, Ü., Keenan, T. F., & Hallik, L. (2015). A worldwide analysis of within-canopy variations in leaf structural, chemical and physiological traits across plant functional types. *New Phytologist*, *205*, 973–993. https://doi.org/10.1111/nph.13096

Niinemets, Ü., Lukjanova, A., Turnbull, M. H., & Sparrow, A. D. (2007). Plasticity in mesophyll volume fraction governs the light-acclimation in needle photosynthesis in two pines. *Tree Physiology*, *27*, 1137–1151. https://doi.org/10.1093/treephys/27.8.1137

Niinemets, Ü., Portsmuth, A., & Tobias, M. (2006). Leaf size modifies support biomass distribution among stems, petioles and mid-ribs in temperate plants. *New Phytologist*, *171*, 91–104. https://doi.org/10.1111/j.1469-8137.2006.01741.x

Niinemets, Ü., & Sack, L. (2006). Structural determinants of leaf-harvesting capacity and photosynthetic potentials. In W. Beyschlag (Ed.), *Progress in botany* (pp. 385–419). Berlin, Germany: Springer Verlag.

Niinemets, Ü., Tobias, M., Cescatti, A., & Sparrow, A. D. (2006). Size-dependent variation in shoot light-harvesting efficiency in shade-intolerant conifers. *International Journal of Plant Sciences*, *167*, 19–32. https://doi.org/10.1086/497845

Niklas, K. J. (1992). *Plant biomechanics: An engineering approach to plant form and function*. Chicago, IL, USA: University of Chicago Press.

Niklas, K. J. (1999). A mechanical perspective on foliage leaf form and function. *New Phytologist*, *143*, 19–31. https://doi.org/10.1046/j.1469-8137.1999.00441.x

Nobel, P. S., Zaragoza, L. J., & Smith, W. K. (1975). Relation between mesophyll surface area, photosynthetic rate, and illumination level during development for leaves of *Plectranthus parviflorus* Henckel. *Plant Physiology*, *55*, 1067–1070. https://doi.org/10.1104/pp.55.6.1067

Oker-Blom, P., Kaufmann, M. R., & Ryan, M. G. (1991). Performance of a canopy light interception model for conifer shoots, trees and stands. *Tree Physiology*, *9*, 221–243.

Oker-Blom, P., & Smolander, H. (1988). The ratio of shoot silhouette area to total needle area in Scots pine. *Forest Science*, *34*, 894–906.

Onoda, Y., Wright, I. J., Evans, J. R., Hikosaka, K., Kitajima, K., Niinemets, Ü., … Westoby, M. (2017). Physiological and structural tradeoffs

underlying the leaf economics spectrum. *New Phytologist*, *214*, 1447–1463. https://doi.org/10.1111/nph.14496

Oren, R., Schulze, E.-D., Matyssek, R., & Zimmermann, R. (1986). Estimating photosynrheric rare and annual catbon gain in conifers from specific leaf weight and leaf biomass. *Oecologia*, *70*, 187–193. https://doi.org/10.1007/BF00379238

Oren, R., Sperry, J. S., Katul, G. G., Pataki, D. E., Ewers, B. E., Phillips, N., & Schäfer, K. V. R. (1999). Survey and synthesis of intra- and interspecific variation in stomatal sensitivity to vapour pressure deficit. *Plant, Cell and Environment*, *22*, 1515–1526. https://doi.org/10.1046/j.1365-3040.1999.00513.x

Osnas, J. L., Katabuchi, M., Kitajima, K., Wright, S. J., Reich, P. B., Van Bael, S. A., … Lichstein, J. W. (2018). Divergent drivers of leaf trait variation within species, among species, and among functional groups. *Proceedings of the National Academy of Sciences*, *115*, 5480–5485. https://doi.org/10.1073/pnas.1803989115

Pickup, M., Westoby, M., & Basden, A. (2005). Dry mass costs of deploying leaf area in relation to leaf size. *Functional Ecology*, *19*, 88–97. https://doi.org/10.1111/j.0269-8463.2005.00927.x

Pittermann, J., & Sperry, J. S. (2006). Analysis of freeze-thaw embolism in conifers. The interaction between cavitation pressure and tracheid size. *Plant Physiology*, *140*, 374–382. https://doi.org/10.1104/pp.105.067900

Pittermann, J., Sperry, J. S., Hacke, U. G., Wheeler, J. K., & Sikkema, E. H. (2006). Inter-tracheid pitting and the hydraulic efficiency of conifer wood: The role of tracheid allometry and cavitation protection. *American Journal of Botany*, *93*, 1265–1273. https://doi.org/10.3732/ajb.93.9.1265

Poorter, H., Niinemets, Ü., Poorter, L., Wright, I. J., & Villar, R. (2009). Causes and consequences of variation in leaf mass per area (LMA): A meta-analysis. *New Phytologist*, *182*, 565–588. https://doi.org/10.1111/j.1469-8137.2009.02830.x

Raupach, M. R., & Thom, A. S. (1981). Turbulence in and above plant canopies. *Annual Review of Fluid Mechanics*, *13*, 97–129. https://doi.org/10.1146/annurev.fl.13.010181.000525

Rodeghiero, M., Niinemets, Ü., & Cescatti, A. (2007). Major diffusion leaks of clamp-on leaf cuvettes still unaccounted: How erroneous are the estimates of Farquhar et al. model parameters? *Plant, Cell and Environment*, *30*, 1006–1022. https://doi.org/10.1111/j.1365-3040.2007.001689.x

Sack, L., Cowan, P. D., Jaikumar, N., & Holbrook, N. M. (2003). The 'hydrology' of leaves: Co-ordination of structure and function in temperate woody species. *Plant, Cell and Environment*, *26*, 1343–1356. https://doi.org/10.1046/j.0016-8025.2003.01058.x

Sack, L., & Frole, K. (2006). Leaf structural diversity is related to hydraulic capacity in tropical rain forest trees. *Ecology*, *87*, 483–491. https://doi.org/10.1890/05-0710

Sack, L., & Holbrook, N. M. (2006). Leaf hydraulics. *Annual Review of Plant Biology*, *57*, 361–381. https://doi.org/10.1146/annurev.arplant.56.032604.144141

Scoffoni, C., Chatelet, D. S., Pasquet-kok, J., Rawls, M., Donoghue, M. J., Edwards, E. J., & Sack, L. (2016). Hydraulic basis for the evolution of photosynthetic productivity. *Nature Plants*, *2*, 16072. https://doi.org/10.1038/nplants.2016.72

Sellin, A., Sack, L., Õunapuu, E., & Karusion, A. (2011). Impact of light quality on leaf and shoot hydraulic properties: A case study in silver birch (*Betula pendula*). *Plant, Cell and Environment*, *34*, 1079–1087. https://doi.org/10.1111/j.1365-3040.2011.02306.x

Sommerville, K. E., Sack, L., & Ball, M. C. (2012). Hydraulic conductance of Acacia phyllodes (foliage) is driven by primary nerve (vein) conductance and density. *Plant, Cell and Environment*, *35*, 158–168. https://doi.org/10.1111/j.1365-3040.2011.02425.x

Sperry, J., Hacke, U., Oren, R., & Comstock, J. (2002). Water deficits and hydraulic limits to leaf water supply. *Plant, Cell and Environment*, *25*, 251–263. https://doi.org/10.1046/j.0016-8025.2001.00799.x

Stenberg, P., Kuuluvainen, T., Kellomäki, S., Grace, J. C., Jokela, E. J., & Gholz, H. L. (1994). Crown structure, light interception and productivity of pine trees and stands. *Ecological Bulletins*, *43*, 20–34.

Stenberg, P., Palmroth, S., Bond, B. J., Sprugel, D. G., & Smolander, H. (2001). Shoot structure and photosynthetic efficiency along the light gradient in a Scots pine canopy. *Tree Physiology*, *21*, 805–814. https://doi.org/10.1093/treephys/21.12-13.805

Thérézien, M., Palmroth, S., Brady, R., & Oren, R. (2007). Estimation of light interception properties of conifer shoots by an improved photographic method and a 3D model of shoot structure. *Tree Physiology*, *27*, 1375–1387. https://doi.org/10.1093/treephys/27.10.1375

Tsuda, M., & Tyree, M. T. (2000). Plant hydraulic conductance measured by the high pressure flow meter in crop plants. *Journal of Experimental Botany*, *51*, 823–828. https://doi.org/10.1093/jexbot/51.345.823

Tyree, M. T., & Ewers, F. W. (1991). The hydraulic architecture of trees and other woody plants. *New Phytologist*, *119*, 345–360. https://doi.org/10.1111/j.1469-8137.1991.tb00035.x

Tyree, M. T., Nardini, A., & Salleo, S. (2001). Hydraulic architecture of whole plants and single leaves. In M. Labrecque (Ed.), *L'arbre 2000 the tree* (pp. 215–221). Montreal, Canada: Isabelle Quentin Publisher.

Vogel, S. (1989). Drag and reconfiguration of broad leaves in high winds. *Journal of Experimental Botany*, *40*, 941–948. https://doi.org/10.1093/jxb/40.8.941

Wear, D. N., & Greis, J. G. (2002). Southern forest resource assessment—Summary of findings. *Journal of Forestry*, *100*, 6–14.

Westoby, M., Falster, D. S., Moles, A. T., Vesk, P. A., & Wright, I. J. (2002). Plant ecological strategies: Some leading dimensions of variation between species. *Annual Review of Ecology and Systematics*, *33*, 125–159. https://doi.org/10.1146/annurev.ecolsys.33.010802.150452

Wong, S., Cowan, I., & Farquhar, G. (1979). Stomatal conductance correlates with photosynthetic capacity. *Nature*, *282*, 424–426. https://doi.org/10.1038/282424a0

Wright, I. J., Dong, N., Maire, V., Prentice, I. C., Westoby, M., Diaz, S., … Leishman, M. R. (2017). Global climatic drivers of leaf size. *Science*, *357*, 917–921. https://doi.org/10.1126/science.aal4760

Wright, I. J., Falster, D. S., Pickup, M., & Westoby, M. (2006). Cross-species patterns in the coordination between leaf and stem traits, and their implications for plant hydraulics. *Physiologia Plantarum*, *127*, 445–456. https://doi.org/10.1111/j.1399-3054.2006.00699.x

Wright, I. J., Reich, P. B., Westoby, M., Ackerly, D. D., Baruch, Z., Bongers, F., … Villar, R. (2004). The world-wide leaf economics spectrum. *Nature*, *428*, 821–827. https://doi.org/10.1038/nature02403

Yang, D., Li, G., & Sun, S. (2008). The generality of leaf size versus number trade-off in temperate woody species. *Annals of Botany*, *2008*(102), 623–629.

Yates, M. J., Verboom, G. A., Rebelo, A. G., & Cramer, M. D. (2010). Ecophysiological significance of leaf size variation in *Proteaceae* from the Cape Floristic Region. *Functional Ecology*, *24*, 485–492. https://doi.org/10.1111/j.1365-2435.2009.01678.x

Zhang, Y. J., Rockwell, F. E., Wheeler, J. K., & Holbrook, N. M. (2014). Reversible deformation of transfusion tracheids in *Taxus baccata* is associated with a reversible decrease in leaf hydraulic conductance. *Plant Physiology*, *165*, 1557–1565. https://doi.org/10.1104/pp.114.243105

Zwieniecki, M. A., Stone, H. A., Leigh, A., Boyce, C. K., & Holbrook, N. M. (2006). Hydraulic design of pine needles: One-dimensional optimization for single-vein leaves. *Plant, Cell and Environment*, *29*, 803–809. https://doi.org/10.1111/j.1365-3040.2005.01448.x

SUPPORTING INFORMATION

Additional supporting information may be found online in the Supporting Information section at the end of the article.

Table S1: Needle length and needle cross-sectional area from published papers.

Table S2: The ratios of circle sector-based estimate circumference ($C_{circle\ sector}$) to measured circumference (C), and of pie-shaped estimate circumference (C_{pie}) to measured circumference (C) in five *Pinus* species (mean ± *SE*, n = 5). The difference between the ratios and 1 were tested using one-sample t-test.

FIGURE S1: Variation in mesophyll phloem fraction (a), xylem fraction (b), vascular bundle fraction (c), transfusion tissue fraction (d), central cylinder fraction (e), epidermal tissue fraction (f) and mesophyll tissue fraction (g) with needle length in five *Pinus* species. Symbols represent species means (n = 5) and error bars represent standard error. PV: *Pinus virginiana*, PEC: *P. echinata*, PT2 and PT1: *P. taeda*, PEL: *P. elliottii*, PP: *P. palustris*.

FIGURE S2: Correlations between circle sector-based circumference, pie-shaped-based circumference and measured circumference with 95% confidence interval in five *Pinus* species. Symbols represent species means (n = 5) and error bars represent standard error. The dotted line demonstrates the 1:1 line. PV: *Pinus virginiana*, PEC: *P. echinata*, PT2 and PT1: *P. taeda*, PEL: *P. elliottii*, PP: *P. palustris*.

FIGURE S3: Light-saturated photosynthetic rate on total needle surface area basis (A_{area}) as a function of stomatal conductance (g_s) (a), and response of g_s (b), and intercellular to ambient CO_2 concentration ratio (C_i/C_a) (c), to leaf-to-air water vapour pressure deficit in five *Pinus* species. Symbols represent individual needle samples (n = 10). Solid line represents relationship with $P < 0.05$, and dotted line represents relationship with $P < 0.10$. PV: *Pinus virginiana*, PEC: *P. echinata*, PT2 and PT1: *P. taeda*, PEL: *P. elliottii*, PP: *P. palustris*.

FIGURE S4: Variation in light-saturated photosynthetic rate on mass basis (A_{mass}) (a), needle N content on mesophyll cells surface area basis ($N_{mesophyll\text{-}surf.}$) (b), and leaf mass per unit of needle length (LML) (c) with needle length in five *Pinus* species. Symbols represent species means (n = 10 for A_{mass}, and n = 5 for $N_{mesophyll\text{-}surf.}$ and LML) and error bars represent standard error. PV: *Pinus virginiana*, PEC: *P. echinata*, PT2 and PT1: *P. taeda*, PEL: *P. elliottii*, PP: *P. palustris*.

How to cite this article: Wang N, Palmroth S, Maier CA, Domec J-C, Oren R. Anatomical changes with needle length are correlated with leaf structural and physiological traits across five *Pinus* species. *Plant Cell Environ*. 2019;42: 1690–1704. https://doi.org/10.1111/pce.13516